Pd SUPPORTED CATALYST FOR GAS-PHASE 1,2-DICHLOROETHANE ABATEMENT: EFFICIENCY AND HIGH SELECTIVITY TOWARDS OXYGENATED PRODUCTS

Z. Boukha, A. Choya, J. González-Prior, B. de Rivas, J.R. González-Velasco, R. López-Fonseca, J.I. Gutiérrez-Ortiz

Journal of Industrial and Engineering Chemistry 57 (2018) 77–88

DOI: 10.1016/j.jiec.2017.08.010

Pd supported catalyst for gas-phase 1,2-dichloroethane abatement: Efficiency and high selectivity towards oxygenated products

Zouhair Boukha, Jonatan González-Prior, Beatriz de Rivas, Juan R. González-Velasco, Rubén López-Fonseca, José I. Gutiérrez-Ortiz

Chemical Technologies for Environmental Sustainability Group,

Department of Chemical Engineering, Faculty of Science and Technology,

University of The Basque Country UPV/EHU,

P.O. Box 644, E-48080 Bilbao, Spain

*Corresponding author: Zouhair Boukha

Phone: +34 946015502

Fax: +34 946013500

E-mail address: zouhair.boukha@ehu.eus

Abstract

Calcium phosphate support (HAP) has been synthesised and impregnated with different amounts of Pd. The prepared Pd/HAP catalysts have been thoroughly characterised by BET, XRD, TEM, UV-visible-NIR, FTIR, XPS, CO_2-TPD and NH_3-TPD techniques and tested in the DCE oxidation reaction.

The characterisation of the catalysts has revealed a clear evolution of the Pd species structure, by increasing the Pd content, from highly dispersed tetrahedral coordinated Pd^{2+} to larger Pd^{2+} species particles adopting square planar geometry. The latter seems to be partially encapsulated by the HAP support.

In DCE oxidation reaction the Pd/HAP system has shown an activity comparable to that of conventional system (Pd/alumina). However, the former has proved high selectivity towards the production of oxygenated products (CO_x (CO_2 and CO)). Notably, in contrast to Pd/alumina, the DCE oxidation does not yield vinyl chloride intermediate product over Pd/HAP. This catalytic behaviour has been related to the moderate acidity of HAP compared to that of alumina together with its interaction with the Pd active phase. This report, then, considers that Pd(x)/HAP could be presented as a good alternative to those reported in the available literature.

Keywords: Pd^{2+} species structure, hydroxyapatite, chemical properties, Cl-VOCs oxidation

1. Introduction

Air pollution caused by the release of volatile organic compounds (VOCs) in different industrial activities is currently considered one of the major environmental problems [1-3]. In this sense, chlorine-containing organic compounds (Cl-VOCs), which are produced in considerable amounts nowadays, require special attention; especially considering their high volatility, toxicity and stability. These chlorinated VOCs, which include polychlorinated methanes, ethanes and ethylenes, are essentially used as cleaning and extraction agents, additives for adhesives and solvents for chemical reactions in a number of industrial processes.

For a long time, thermal incineration has been employed as an effective remediation technology for the removal of Cl-COVs. There are, however, a number of drawbacks that strongly restrict the application of traditional incinerators as they require high operation temperatures and release undesirable by-products [1-3]. For this reason, in the last few decades, research has focused on the development of catalytic processes that could allow operating at low temperatures in order to decrease the processing cost and NO_x emissions. Recently, much effort has been devoted to the development of catalytic systems for hydrodechlorination processes to transform Cl-VOCs to unsaturated hydrocarbons with high added value [4-9]. However, the economic viability of this strategy, which involves hydrogen consumption and a demanding catalyst activation step, lacks evidence to be considered as an alternative. By contrast, catalytic oxidation of Cl-VOCs is still considered as a method of choice because it allows the oxidation to proceed at low temperatures and results in a diminution of NO_x emissions [1-3]. Moreover the use of efficient catalysts can increase the selectivity towards deep oxidation products (CO_2 and HCl) at the expense of undesirable products, such as CO, vinyl chloride (VC) and Cl_2.

Generally, catalysts for Cl-VOCs oxidation consist of transition metal oxides (Co, V, Cr, Mn) and supported noble metal (Pt, Pd, Ru and Rh) catalysts [1-3, 10-16]. Despite their low cost, the application of transition metal oxides is strongly limited, due to the formation of volatile metal oxychlorides, which promote the loss of the active phase [17]. By contrast, in accordance with experimental studies carried out on a wide series of Cl-VOCs oxidation catalysts, noble metals showed high resistance against volatilization and exhibit higher specific activity compared to those of metal oxides [18]. Though a number of reports dealing with different noble metal catalysts are presently available, due to their high activity and thermal stability supported Pd catalysts are by far the most investigated systems. For instance, Gonzalez-Velasco et al. [3] compared the behaviour of Pd and Pt catalysts and reported that Pd/alumina was more active and less selective to produce Cl_2 than Pt/alumina in 1,2-dichloroethane (DCE) and trichloroethylene (TCE) oxidation, under rich-oxygen conditions. On the other hand, it is known that, in the Cl-VOCs oxidation, the nature of the support plays a key role in the catalytic properties of the supported Pd catalysts and in their stability [1]. For this reason, current research is dedicated to the synthesis of supports exhibiting suitable physico-chemical properties in order to overcome the main problems related to deactivation of Pd catalysts, namely sintering, chlorine adsorption and coke deposition. For this purpose, various supports (including Al_2O_3, zeolites, SiO_2, CeO_2, La_2O_3, ZrO_2-TiO_2) have been used to disperse the Pd species and to generate new interactions which might enhance their activity, selectivity and stability [1,19-22]. Special attention has been paid to determine the influence of the nature of acid sites of the support because of their key role in the activity and the products distribution [19-22].

Among the promising non-classic supports hydroxyapatite material (HAP: $Ca_{10}(PO_4)_6(OH)_2$) has attracted increasing interest in the last decades [2,23-25]. This is

due to its high structural flexibility which allows different substitutions and ion exchanges. Moreover, the surface chemical properties of HAP can be substantially modulated by varying the Ca/P ratio. Recently, in our study devoted to examine the catalytic behaviour of Pd/HAP catalysts in various CO elimination processes [23], we found that their performance evidenced the potential of HAP support as good alternative to the classical supports. Moreover, in relation with the Cl-VOCs abatement, we studied the applicability of Co/HAP catalysts in the oxidation of DCE [2]. Due to a significant enhancement of the textural and structural properties the resulting Co/HAP catalysts achieved a higher activity compared to bulk Co_3O_4, thereby confirming the advantage of dispersing cobalt on a relatively high surface area HAP.

In the present work, we investigate the applicability of a non-stoichiometric hydroxyapatite (Ca/P = 1.50) as a porous support of the Pd species in the total oxidation of DCE. The choice of such composition was made in order to obtain an active surface bearing more acidic sites [26], as suitable chemical properties for the oxidation of Cl-VOCs, compared with stoichiometric hydroxyapatite (Ca/P = 1.67). Interesting conclusions have been drawn from the correlation between the physicochemical properties of Pd/HAP samples, determined by different characterisation techniques (including BET, TEM, XRD, FTIR, UV–VIS-NIR DRS, XPS spectroscopy and volumetric adsorption of NH_3 and CO_2), and their performance in the DCE oxidation reaction. Special attention will be devoted to the catalyst structure changes and their impact on the efficiency of palladium in the reaction.

2. Experimental

2.1. Preparation of the catalysts

Calcium-deficient hydroxyapatite support (HAP), with Ca/P molar ratio equal to 1.50, was synthesized adding drop wise a boiled aqueous solution of calcium nitrate to a solution of $(NH_4)_2HPO_4$. The precipitate was re-dissolved in a nitric acid solution and neutralized with ammonia at pH of 10-11. The resulting mixture was maintained under stirring at 80 °C for 16 h. After filtration, the recovered solid was washed well with purified water, until the pH of the filtrate reached a value of 7, then dried at 120 °C and finally calcined at 500 ºC for 4 h.

The Pd(x)/HAp catalysts (0.5 wt.% ≤ x ≤ 2 wt.%) were prepared by impregnation of the HAP support by tetraamminepalladium (II) chloride monohydrate. The prepared catalysts were dried at 120 ºC for 12 h and, then, calcined at 500ºC for 4h.

2.2. Characterisation techniques

The volumetric N_2 adsorption at -196 °C was performed on an automatic apparatus Micromeritics, model TRISTAR II 3020 apparatus. The pre-treatments applied to the samples consisted of a cleaning, at 300 °C (overnight), under nitrogen flow. The specific areas of the samples were determined in line with the standard BET procedure, using nitrogen adsorption taken in the relative equilibrium pressure interval of 0.03-0.3.

X-ray diffraction (XRD) studies were conducted on a X'PERT-MPD X-ray diffractometer with Cu Kα radiation (λ = 1.5406 Å) and Ni filter. The X-ray tube was operated at 40 kV and 40 mA. The samples were scanned between 10° and 100° (2θ), and the X-ray diffraction line positions were determined with a step size of 0.01° and a counting time of 2.5 s per step. Phase identification was conducted by comparison with JCPDS database cards.

Fourier transform infrared spectroscopy (FTIR) absorption spectra were recorded in the 400-4000 cm^{-1} range with a Cary 600 Series FTIR spectrometer using disks of samples diluted in KBr.

The oxidation states and the coordination of the Pd species were investigated by diffuse reflectance UV-visible-NIR spectroscopy (UV-visible-NIR DRS) with a UV-vis-NIR Cary 5000 apparatus coupled to Diffuse Reflectance Internal 2500 within a range of 200-2500 nm. The PdO absorption edge was determined according to a procedure previously described by Weber [27]. The position of absorption edges were determined for allowed transitions by finding the energy intercept of a straight line fitted through the low energy rise in the graph of $[F(R) \times h\nu]^2$ vs $h\nu$, where F(R) is the Kubelka-Munk function and $h\nu$ is the incident photon energy.

The morphology, size and dispersion of the palladium particles were examined by transmission electron microscopy (TEM). The TEM studies were performed on a Philips CM200 transmission electron microscope equipped with LaB6 filament operating at 200 kV and combined with X-ray energy dispersive spectroscopy (X-EDS) techniques.

The temperature programmed desorption of CO_2 studies (CO_2-TPD) were carried out on a Micromeritics AutoChem 2920 instrument coupled to a MKS Cirrus LM99 mass spectrometer. The catalysts were submitted to a pre-treatment consisting on their heating at 500 ºC (30 min) in a flow 5%O_2/He (50 cm^3 min^{-1}) and cooling to 40 °C in a flow of He. The adsorption of CO_2 was performed in a flow of 10%CO_2/He (50 cm^3 min^{-1}) for 30 min. After CO_2 adsorption the samples were treated with He for 2 h and heated at 10 ºC min^{-1} up to 500 ºC in flowing He (50 cm^3 min^{-1}).

The acid properties of the catalysts were determined by temperature programmed desorption of NH_3 (NH_3-TPD). The samples were submitted to the same experimental

conditions used for CO_2-TPD. The adsorption of NH_3 was performed in a flow of 10%NH_3/He (50 cm^3 min^{-1}) for 30 min. The NH_3 signal (m/z=15) was analysed online by mass spectrometry.

On the other hand, the amount of carbonaceous deposits on the used catalyst (40 mg) was determined by temperature programmed oxidation (TPO-MS) on the same experimental setup used for CO_2-TPD experiments coupled to a MKS Cirrus LM99 mass spectrometer. A flow 5%O_2/He (50 cm^3 min^{-1}) was used as an oxidant stream. The temperature was increased from 40 to 900 °C at a constant heating rate of 20 °C min^{-1}.

2.3. Catalytic tests

Catalytic tests were performed in a bench-scale fixed bed reactor operated at atmospheric pressure. The reactor was made of quartz with an internal diameter of 10 mm and a height of 300 mm, in which the temperature is controlled with a thermocouple placed in the catalyst bed. Typically 0.85 g of catalyst in powdered form (0.3-0.5 mm) was loaded. The reaction feed consisted of 1000 ppm of DCE in dry air with a total gas flow of 500 cm^3 min^{-1} (15,000 h^{-1}). It should be noted that the experimental conditions employed in this work were chosen to meet the criteria to ensure the absence of the mass and heat transfer limitations, as described elsewhere [28]. Catalytic activity was measured over the range 150-500 °C and conversion data were calculated by the difference between inlet and outlet concentrations. Conversion measurements and product profiles were taken at steady state, typically after 30 min on stream.

The feed and effluent streams were analysed using an on-line 7980A Agilent Technologies gas chromatograph equipped with a thermal conductivity (CO and CO_2) and an electron capture detector (chlorinated hydrocarbons). Analysis of HCl and

Cl_2 was carried out by means of ion selective electrode and titration, respectively. Further details on analytical procedures can be found elsewhere [28]. On basis of the concentrations [C_i] at the outlet and the inlet of the reactor, DCE conversion to CO_x (X_{DCE}) and selectivity towards CO and CO_2 were calculated, according to the following equations:

$$X \qquad \text{(1)}$$

$$\text{(2)}$$

$$\text{(3)}$$

Turnover frequency (TOF) values were calculated as the activity data per mole of palladium. In order to assure differential reactor conditions the temperatures used for the calculations of TOF over the Pd(x)/HAP catalysts corresponded to low DCE conversions.

3. Results and discussion

3.1. Catalytic activity of the Pd(x)/HAP samples in the DCE oxidation

The DCE oxidation reaction has been examined over the Pd(x)/HAP catalysts in the temperature window between 150 and 500 °C, by sequentially increasing the reaction temperature with 25 °C intervals. Fig. 1 displays the evolution of DCE conversion (X_{DCE}) over the Pd(x)/HAP catalysts versus reaction temperature. Over the bare HAP support the reaction begins around 225 °C and the conversion increases slowly up to 375 °C. Then it starts to increase rapidly with reaction temperature, but it does not exceed 48% at 500 ºC. Fig. 1 also shows that the addition of palladium promotes the

DCE oxidation activity. Indeed, over the three Pd catalysts the reaction ignition starts at 200 °C and the conversion increases rapidly with the temperature to reach a conversion close to 100% at 450 ºC over the Pd(0.5)/HAP and Pd(1)/HAP catalysts; whereas, the Pd(2)/HAP catalyst reaches its maximum conversion (93%) at 500 ºC. Table 1 compares the obtained results in terms of the temperatures at which the DCE conversion reaches 10% (T_{10}), 50% (T_{50}) and 90% (T_{90}). The temperatures required for 10% and 50% DCE conversion do not seem to be affected by the Pd loading (275-280 ºC and 342-352 ºC, respectively). However, the Pd(2)HAP catalyst presents the highest T_{90} (450 ºC) compared to the low Pd loading catalysts (415 ºC for Pd(0.5)/HAP and 410 ºC for Pd(1)/HAP).

Table 1 also lists the specific activity values in terms of $mol_{DCE}\ g^{-1}\ s^{-1}$, $mol_{DCE}\ m^{-2}\ s^{-1}$ and $mol_{DCE}\ mol_{Pd}^{-1} s^{-1}$ (TOF) determined for a conversion lower than 20% (at 275 ºC). The analysis of the obtained values evidences the superiority of the Pd(0.5)/HAP catalyst. For instance, TOF significantly decreases with the Pd loading from 10.1×10^{-4} s^{-1} for the Pd(0.5)/HAP sample to 5×10^{-4} s^{-1} and 2×10^{-4} s^{-1} for Pd(1)/HAP and Pd(2)/HAP, respectively. Furthermore, the apparent activation energy (Ea) for the Pd(x)/HAP catalysts is calculated assuming a first order reaction. As reported in Fig. 2 a linear correlation is obtained between $\ln[-\ln(1-X_{DCE})]$ and 1/T. According to the data reported in Table 1 the lowest activation energy value, 59.2 kJ mol^{-1}, is obtained for the Pd(0.5)/HAP catalyst whereas it is significantly higher, 69.8-70.6 kJ mol^{-1}, over the Pd(1)/HAP and Pd(2)/HAP catalysts. The analysis of the E_a and TOF values trends points out that the activation of the DCE molecule might be sensitive to the nature of the Pd active species that are deposited on each catalyst. In this sense, the lowest E_a and the highest TOF values obtained on the Pd(0.5)/HAP sample can be attributed to the presence of the most active species of Pd.

Fig. 3 (a-d) shows the concentration-temperature profiles of the main oxidation products (CO_2, CO, VC and HCl, respectively). On the bare HAP support, the formation of CO_2 is very low (< 150 ppm) in all the reaction temperatures range (up to 500 ºC) (Fig. 3a). However, the addition of palladium increases notably the selectivity towards CO_2 production. Indeed, at 500 ºC, 1950 ppm of CO_2 are produced on the Pd(0.5)/HAP and Pd(1)/HAP catalysts and 1750 ppm are produced over Pd(2)/HAP catalyst. Regarding the CO production it can be observed that, over the Pd catalysts, it increases rapidly, compared to the CO_2 profile, before reaching a maximum around 950-1050 ppm at 375 ºC (Fig. 3b). Above this temperature, CO_2 production predominates due to CO oxidation. By contrast, on the HAP support the concentration of the produced CO increases continuously with the temperature to reach 800 ppm at 500 ºC. Many reports on a wide variety of supported and unsupported catalysts pointed out that the low selectivity to CO_2 observed at low temperatures could be related to a possible chlorination of the catalyst which inhibits the oxidation of carbon monoxide [1,29-33]. Fig. 3c shows the production profiles of HCl. Generally, HCl is the preferred chlorinated product because it can be easily trapped by aqueous scrubbing [1-2]. As it can be seen in Fig. 3c hydrogen chloride is the main deep DCE oxidation product over the Pd catalysts. The shape of its production profiles is quite similar to that of DCE conversion enclosing all the temperatures range corresponding to the yield of both CO and CO_2. At 500 ºC, the highest concentration of HCl (1900 ppm) is detected on the Pd(0.5)/HAP catalyst. This maximum value slightly decreases at higher palladium contents (1850 ppm over Pd(1)/HAP and 1700 ppm over Pd(2)/HAP). It should be noted that the Pd(x)/HAP system does not favor the occurrence of the Deacon reaction. Indeed, very small amounts of Cl_2 (< 75 ppm) are detected, at temperatures higher than 450 ºC, over all the investigated samples.

The HAP support effect on the selectivity was also studied following the VC intermediate product (Fig. 3d). The VC production trace corresponding to the bare support is characterised by the presence of a peak centred at 425 °C (800 ppm) before decreasing sharply for T > 425 °C with high CO production, as above commented. Nevertheless, the VC intermediate product disappears completely, in all the explored temperatures, with the addition of Pd. This observation points out that the use of hydroxyapatite as support for Pd catalysts is not selective towards the production of VC intermediate product. In this sense, these results show remarkable differences with respect to those reported in previous studies on the activity of Pd catalysts in the Cl-VOCs oxidation [20,29-30]. Over the latter, considerable amounts of chlorinated intermediate molecules were detected as undesirable products. For instance, over a Pd/alumina catalyst the DCE oxidation produces vinyl chloride with a maximum centred at 350 ºC [29]. Also, it was found that the oxidation of trichloroethylene (TCE) on the Pd/alumina and Pd/zeolites catalysts produces considerable amounts of tetrachloroethylene [20,31]. Generally, the production of these intermediate products occurs at mild temperatures and their high selectivity is principally related with the presence of strong surface acid sites [20,29-33]. On the mechanism that describes the reaction steps over Pd catalysts Aranzabal et al. [29] concluded that DCE is first decomposed by dehydrochlorination to VC and HCl, followed by direct oxidation to CO and CO_2. Accordingly, we conclude that over our Pd(x)/HAP catalysts the oxidation step is fast enough to convert immediately the VC intermediate product to HCl, CO and CO_2.

It worth mentioning that, over the Pd catalysts, carbon balances are slightly higher than 100% at elevated temperatures (325-500 ºC) which may be due to the combustion of the coke formed at lower temperatures. TPO-MS analyses effectively show that very small

amounts of carbon are accumulated on the used catalysts (< 0.5 wt.%). On the other hand, a surface semi-quantitative analysis of the post-reaction catalysts was conducted by X-EDS techniques; particularly focused on the determination of chlorine species amounts deposited on their near surface. The results reveal that the amount of accumulated chlorine on all the post-reaction samples is ranged between 5-6 wt.%. These values are somewhat close to that expected for a stoichiometric chlorapatite structure (6.8%). The chlorination phenomenon was reported in previous works dealing with the oxidation of Cl-VOCs over various Pd systems and attributed to the interaction of chlorine with both the support and the metal active phase [1-2, 20, 34-35]. In order to assess the impact of the chlorination on the catalytic stability additional experiments are carried out at 375 ºC during a relatively prolonged time on stream, 68 hours, over the most active catalyst (Pd(0.5)/HAP). As shown in Fig. 4, this catalyst exhibits a stable performance in terms of DCE conversion and selectivity toward CO and CO_2 products which suggest a low impact of induced chlorination.

3.2. Characterisation of the samples

3.2.1. N_2-physorption (BET measurements)

The textural properties of the Pd(x)/HAP catalysts were examined by nitrogen adsorption-desorption measurements. The corresponding isotherms (not displayed) show that they are characteristic of mesoporous materials exhibiting IV-type according to the IUPAC classification. The specific surface area, pore volume and average pore size are listed in Table 2. As deduced from the reported data the addition of palladium (0.5-2%) to HAP (52 m^2 g^{-1}) causes a slight drop in the specific surface area (7.5%) and pore volume. Table 2 also lists the textural properties corresponding to the post-reaction samples. Hence, the bare support shows an apparent drop in its specific surface area

(about 11.5%) after the catalytic test. This result is reasonably consistent with a possible phase transformation of hydroxyapatite, to be commented below, which may accelerate the loss of its surface area. Furthermore, in contrast to the Pd(0.5)/HAP and Pd(1)/HAP, which keep their textural properties, the catalyst with higher Pd loading (Pd(2)/HAP) suffers a significant loss (14.6%) in its specific surface area (Table 2).

3.2.2. Transmission electron microscopy (TEM)

TEM images of the Pd particles deposited on the calcined Pd(x)/HAP catalysts are shown in Fig. 5. As reported in Fig. 5a Pd species nuclei, with sizes lower than 5 nm and exhibiting weak contrast and different shapes, are formed on the Pd(0.5)/HAP sample. At higher Pd loadings (1% and 2%) there is an apparent increase in the Pd species particle sizes (Fig. 5b and Fig. 5c.). In both cases darker particles are observed with a mean size of 10 nm for Pd(1)/HAP and 18 nm for Pd(2)/HAP. This suggests that, for the Pd-rich samples, the palladium distribution starts to be modified, when compared to that of Pd(0.5)/HAP. The occurrence of nanometer-sized particles might thus be interpreted as an indication of the evolution from highly dispersed particles to an initiation of local concentration of palladium and a tridimensional growth of its crystals. Figs. 5d and 5e show HRTEM images of an isolated PdO particle for the Pd-rich sample catalyst. On the particle centre an apparent overlap of the PdO and HAP crystalline planes, forming moire fringes, can be appreciated. The estimations of different lattice spacing evidence the presence of, at least, three distinct reflections corresponding to distances of ~0.23 nm, ~0.3 nm and ~0.8 nm. The latter value could be associated with (100) reticular plane of hydroxyapatite structure which has a theoretical value of 0.8151 nm (JCPDS 01-082-2956). However, because of both PdO ($P4_2/mmc$) and HAP ($P6_3/m$) structures have a set of reflections with spacing between 0.2-0.3 nm,

it is difficult to distinguish their corresponding lattice spacing. According to PdO JCPDS cards (41-1107), in the spacing range of 0.2-0.3 nm, PdO structure presents four reflections [(100): 0.305 nm, (002): 0.266 nm, (101): 0.264 nm and (110): 0.215 nm] while HAP structure presents sixteen different reflections. Nevertheless, interestingly, on the basis of the different contrast between the two matrices, Figs. 5d and 5e evidence the presence of HAP layer (low contrast) surrounding a PdO large particle. These observations point out, at least, a partial encapsulation of the latter by HAP support. In line with our proposal, in their study on a Pd/SiO_2 catalyst, Forman et al. [42] found that large Pd particles were susceptible to be encapsulated, compared to the smaller ones. The partial encapsulation of metal particles by different oxide supports, under certain conditions, can also be found in many reports [44-45]. For instance, in their study on the Pd/CZ catalysts, Sun et al. [45] attributed the encapsulation of the Pd particles to a compressive stress in the top layer of the CZO surface which led to a diffusion of oxide cations and anions along the CZO surface toward Pd particles, causing their partial encapsulation.

3.2.3. X-ray diffraction (XRD)

Fig. 6 displays the powder XRD patterns for the Pd(x)/HAP samples. Pure HAP exhibits the characteristic peaks of a hexagonal structure with the space group $P6_3/m$ (JCPDS 01-082-2956). As expected, due to the non-stoichiometry of our HAP sample (Ca/P=1.50) its 2θ angles values corresponding to the main diffraction peaks 26.2°, 32.0°, 32.4°, 33.2°, 34.3°, 40.1º, 47.0º and 49.7º are slightly higher than those corresponding to stoichiometric hydroxyapatite (25.9º, 31.8º, 32.2º, 32.9º, 34.1º, 39.8º, 46.7º and 49.5º). On the XRD pattern of the Pd(0.5)/HAP sample no peak due to PdO species is observed probably because of their high dispersion and/or their small

amounts. By contrast, the diffractograms of the high Pd loading samples (1% and 2%) exhibit a shoulder around 33.9º, corresponding to (101) main reticular plane, which can be attributed to palladium oxide structure (PDF 43-1024). Table 3 lists the lattice parameters of the HAP structure calculated for all the analysed samples. The reported data show that the parameter "a" and unit cell volume increase with increasing the Pd content which suggests an incorporation of Pd in the HAP crystal lattice. Similar observation can be found in our previous study dealing with reduced Pd(x)/HAP samples [23]. By combining the information obtained from XRD and temperature-programmed reduction studies we had proposed a possible incorporation of 0.3% Pd, as an upper limit, into the hydroxyapatite network.

On the other hand, according to Fig. 6, the XRD analyses of the post-reaction catalysts reveal the disappearance of the hydroxyapatite phase which is transformed into its chlorinated analogue (Chlorapatite: $Ca_{10}(PO_4)_6Cl_2$). The diffractogram of the latter is characterised by two intense peaks centred at $2\theta = 31.5°$ and 32.4° (JCPDS: 027–0074). Similar observations concerning the phase transformation of hydroxyapatite were found in our previous study on the Co/HAP catalysts used in DCE oxidation reaction [2]. Nevertheless, due to the XRD techniques limitations (small Pd amounts and/or highly dispersed Pd species), the diffractograms of the spent Pd(x)/HAP catalysts show no lines corresponding to Pd species. As will be shown later the possible Pd structures on the spent catalysts can be identified by spectroscopic measurements.

3.2.4. Fourier transform infrared spectroscopy (FTIR)

Fig. 7 includes the FTIR spectra for HAP and Pd(x)/HAP catalysts. The spectrum corresponding to HAP support is characteristic of the molecular vibrations of phosphates and hydroxyls groups by the hydroxyapatite framework. The different

vibrational modes of P-O bonds that attest the presence of $(PO_4)^{3-}$ groups exhibit five bands centred at 566, 602, 960, 1035 and 1095 cm^{-1} [2, 24-25]. Moreover, the presence of a small sharp band at 3575 cm^{-1} and a more intense feature at 630 cm^{-1} are attributed to the hydroxyls groups [2, 24-25]. It should be noted that, as expected, in agreement with the ICP results, the spectrum of HAP sample presents a band around 875 cm^{-1}, which confirms the presence of $(HPO_4)^{2-}$ ions, typical of calcium deficient hydroxyapatite ($Ca_{10-z}(HPO_4)_z(PO_4)_{6-z}(OH)_{2-z}$). On the spectrum of the low Pd catalyst (Pd(0.5)/HAP) there are no changes with respect to that of the bare support. However, new shoulders appear at higher Pd loadings (1% and 2%) which affect the absorption of the water molecule vibrations in the 3200-3600 cm^{-1} range. On the basis of previous studies this behaviour evidences a growth of supported metal particles which interact with water molecules [2,36].

3.2.5. UV-visible-NIR diffuse reflectance spectroscopy (UV-visible-NIR DRS)

The optical properties of the Pd species deposited on the prepared Pd(x)/HAP catalysts are examined by means of UV-visible-NIR DRS techniques. Fig. 8a displays the optical absorption spectra recorded in the range 200-2500 nm. The attribution of the absorption bands is carried out by comparison with spectra of earlier studies dealing with palladium complexes. The spectrum of the bare support is characterised by the presence of several bands ranged between 1200-2200 nm, NIR region, assigned to hydroxyl groups. Moreover, the UV domain exhibits a maximum around 200 nm ascribed to ligand-to-metal charge transfers ($O^{2-} \rightarrow Ca^{2+}$) [2,25].

As expected, the addition of palladium results in new bands in the UV-visible domain. It should be noted that, as the concentration of Pd increases, the samples colour change from brown-green for Pd(0.5)/HAP to brown for Pd(1)/HAP and dark brown in the case

of Pd(2)/HAP. The spectrum of the low Pd loading sample, Pd(0.5)/HAP, exhibits two additional bands at 220 nm and 420 nm ascribed to $O^{2-} \rightarrow Pd^{2+}$ charge transfers and to d-d transitions of Pd^{2+} in tetrahedral coordination, respectively [37]. The increase of Pd concentration red-shifts the charge transfer band from 220 nm to 285 nm and produces a splitting of the band at 420 nm into two bands centred at 360 and 450 nm (Fig. 8a). These observations point out that the progressive addition of Pd induces a structure evolution of the Pd^{2+} species from tetrahedral to square planar geometry (D_{4h}) [37]. According to XRD and TEM data, the former may be associated with strongly interacting species of Pd with HAP support.

On the other hand, due to their p-type semiconductor character, the particle sizes of the PdO species could be correlated with the width of their band gaps [38-39]. For example, narrow band gap indicates the presence of relatively large particles (> 20 nm) as in the case of bulk PdO whose absorption threshold lies in the NIR, 0.6-0.8 eV (1550-2070 nm) [38]. For all the Pd(x)/HAP catalysts the band gap lies in the visible domain, 1.9-2.1 eV (590-650 nm), pointing out that, in good agreement with the TEM results, the PdO species are deposited as nanosized particles (< 20 nm).

Fig. 8b shows the UV-visible-NIR spectra of the Pd(x)/HAP post-reaction catalysts. The spectrum of the Pd(0.5)/HAP sample exhibits two bands, in the UV region, at 225 nm and 280 nm attributed to ligand-metal charge transfer transitions. Moreover, the Pd(0.5)/HAP spectrum show a well-resolved band at 475 nm and a shoulder at 325 nm, ascribed to allowed d-d transitions. It is worth mentioning that this set of the four UV-visible bands were also observed by Sales et al. [38] in their $PdCl_2$ solution spectrum and they assigned them to the $(PdCl_4)^{2-}$ complexes in D_{4h} symmetry. The formation of the latter on the used Pd(0.5)/HAP sample can reasonably explain its colour change from brown-green to orange. These results confirm the chlorination of surface

palladium species by adsorbed chlorine associated with the destruction of 1,2-dichloroethane molecules. Interestingly, besides the $(PdCl_4)^{2-}$ complex bands, the used Pd-rich sample spectrum, Pd(2)/HAP, shows that the characteristic PdO bands are still present; especially the band centred at 450 nm. In view of this relevant observation it can be concluded that, in contrast to the Pd(0.5)/HAP catalyst, two Pd species coexist on the higher Pd loading catalysts (PdO and $(PdCl_4)^{2-}$ complexes). This suggests, thus, that the Pd chlorination process concerns only the surface Pd species. It should be noted that these results are in good agreement with TEM results. The presence of encapsulated Pd particles makes them inaccessible to the gas mixture and, then, less susceptible to be chlorinated.

3.2.6. X-ray photoelectron spectroscopy (XPS)

The chemical composition and the distribution of Pd species laying on the surface of the calcined Pd(x)/HAP catalysts are investigated by means of XPS techniques. Fig. 9 and Table 3 summarise the corresponding results.

According to Fig. 9 and Table 3, all the Pd catalysts exhibit a typical Pd $3d_{5/2}$ peak close to 336.7 ± 0.3 eV assigned to PdO particles [40,41]. However, the position of this feature seems to depend on the Pd content. Hence, for low Pd loadings (≤ 1%) the observed peak is centred at 337 eV; whereas it shifts towards lower binding energies in the case of the Pd-rich sample (336.4 eV). According to many reports this trend could be attributed to a decrease in the oxidation state of palladium oxide [40,41]. Since small particles are easier to oxidise compared to large ones, these results agree well with the TEM data. The latter show that larger Pd particles are deposited on the Pd(2)/HAP (18 nm) compared to Pd(1)/HAP (10 nm) and Pd(0.5)/HAP (5 nm).

Upon integration of the Pd $3d_{5/2}$, Ca 2p and P 2p spectra, the corresponding Pd/P and Ca/P atomic ratios could also be estimated. As deduced from Table 3 these ratios exhibit significant differences with respect to those determined by ICP techniques. For instance, for all the Pd catalysts the surface Ca/P ratio (XPS) seems to be lower than that estimated by bulk analysis (ICP). This loss in calcium is more pronounced on the Pd(0.5)/HAP sample which exhibits an important decrease in its Ca/P ratio from 1.48 (ICP) to 1.39 determined by XPS. On the same sample the Pd/P ratio remains almost constant. These observations point out an apparent enrichment of the near surface with Pd. By contrast, at high Pd loadings (1% and 2%) the $(Pd/P)^{XPS}$ ratio seems to be lower than $(Pd/P)^{ICP}$ suggesting an apparent loss in palladium on the catalysts near surface. This loss in surface palladium amounts occurred in the Pd-rich samples is very consistent with the TEM results which indicated an apparent growth of the Pd particles and their encapsulation by HAP support.

3.2.7. Acid-base properties of the Pd(x)/HAP catalysts

The surface basicity of the Pd(x)/HAP catalysts was characterised by means of CO_2-TPD techniques. Fig. 10 shows the corresponding desorption profiles recorded on the samples after pre-adsorption of CO_2 at 40 °C for 1 h. The amounts of desorbed CO_2 extracted from the integration of the observed desorption bands are reported in Table 4. Data corresponding to the bare HAP are also included for comparison.

According to Fig. 10 and Table 4 the dispersion of palladium onto the HAP surface dramatically decreases both the amount and thermal stability of the adsorbed CO_2. The specific basicity of the HAP (2.6 $\mu mol_{CO2}\ m^{-2}$) seems to decrease linearly with the increase of the Pd content (1.5 $\mu mol_{CO2}\ m^{-2}$ for Pd(0.5)/HAP, 1.2 $\mu mol_{CO2}\ m^{-2}$ for Pd(1)/HAP and 0.7 $\mu mol_{CO2}\ m^{-2}$ for Pd(2)/HAP). Moreover, the addition of Pd affects

the distribution of basic sites. The CO_2-TPD trace for HAP support shows that, besides the weak-medium strength basic sites (peaked at T ≤ 300 ºC), it bears a significant amounts of strong basic sites peaked at 350 ºC. By contrast, a narrower distribution is observed in the presence of palladium, essentially characterised by an absence of the peak at 350 ºC, suggesting an apparent weakening of the surface basic sites. In their study on the properties of hydroxyapatites with various compositions Silvester et al. [43] proposed that the absence of the peak due to stronger basic sites arises from the lack in basic OH^- ions. In accordance with our FTIR results, we think that in our Pd(x)/HAP system the deposition of palladium leads to a dehydroxylation of the support which decreases the strength of its basic sites.

The acid properties of the catalysts are investigated by means of NH_3-TPD. Fig. 11 shows the corresponding diagrams for all the prepared catalysts. The profile of the HAP support consists of an asymmetric desorption peak with a maximum at 180 ºC. The addition of palladium results in broader desorption window and shift its maximum to relatively higher temperatures (190-215 ºC). This implies that the presence of palladium leads to an apparent increase in the strength of the acid sites. Table 4 includes the acid sites density values determined from the integration of the NH_3-TPD curves. The surface density of NH_3 adsorption sites on HAP support is 1.7 μmol m^{-2}. The latter value shows that HAP support exhibits low surface acid density compared to that of alumina support (4.7 μmol m^{-2}). The introduction of 0.5% of Pd significantly decreases the density of the acid sites which reaches a value of 1.3 μmol m^{-2}. However, values close to that determined for HAP support are estimated on the high Pd loadings (1.5 μmol m^{-2} for both Pd(1)/HAP and Pd(2)/HAP catalysts). In good agreement with the XPS and TEM data, these results could be explained by a decrease in the fraction of the

exposed Pd, due to its encapsulation, where the support surface acidity seems to be dominant.

3.3. Discussion

In accordance with the conclusions drawn from the characterisation studies and catalytic tests in the DCE oxidation, it is worth analysing the interest of Pd(x)/HAP samples as alternative catalysts to those reported in the available literature. Though the overall activity shown by our Pd(x)/HAP catalysts are quite similar to that of Pd/alumina catalysts, reported by Aranzabal et al. [29], the selectivity of the reaction products shows remarkable differences. Essentially, our Pd(x)/HAP system proves that it is highly selective towards CO_x (CO_2 and CO) and HCl production compared to Pd/alumina. Over the latter, considerable amounts of VC were produced which lowers the selectivity towards both CO_x and HCl production [29]. Since the production of VC intermediate molecule is mainly attributed to the acidity of the support we think that the difference between HAP and alumina mainly consists of the number of acid sites lying on the surface. Despite the former has a sub-stoichiometric Ca/P molar ratio (1.39-1.50) it still exhibits a moderate acidity when compared to that of alumina. These chemical properties together with the interaction of Pd active phase with HAP support seem to be determinant factors in enhancing the selectivity towards oxygenated products (CO and CO_2).

Regarding the effect of the Pd loading on the activity of Pd(x)/HAP, a notable decrease in TOF values, at 275 ºC, from 10.1 x 10^{-4} mol_{DCE} $mol_{Pd}^{-1}s^{-1}$, for Pd(0.5)/HAP, to 5 x 10^{-4} mol_{DCE} $mol_{Pd}^{-1}s^{-1}$, for Pd(1)/HAP, is found. The Pd-rich sample (Pd(2)/HAP) is even less active, exhibiting the lowest TOF value, 2 x 10^{-4} mol_{DCE} $mol_{Pd}^{-1}s^{-1}$. This behaviour could be explained by the presence of more efficient species at low Pd

loading. As revealed by UV-visible-NIR techniques, there is a clear evolution in the structure of Pd species from highly dispersed tetrahedral coordinated Pd^{2+} to larger Pd^{2+} species particles adopting square planar geometry. When correlated with XRD data one can claim that these results imply that the former corresponds to the fraction of Pd which incorporated the HAP framework. TEM and XPS results, however, evidence an occurrence of encapsulated and inactive fraction of palladium at high loadings.

In parallel with the structural changes of the Pd species, the NH_3 volumetric adsorption studies show that the presence of highly dispersed Pd species decreases the density of surface acid sites. The characterisation of the spent catalysts points out that the active phase in DCE oxidation consists of the strongly interacting Pd^{2+} species and the HAP phases. As revealed by UV-visible-NIR and XRD, their activity is accompanied by their transformation to $(PdCl_4)^{2-}$ complex and chlorinated apatite, respectively. The activity of Pd(0.5)/HAP, however, does not seem to be affected by these chlorination processes. By contrast, due to their inactivity and inaccessibility to the gas mixture, the encapsulated Pd particles keep their structure intact.

4. Conclusions

Calcium-deficient hydroxyapatite support (HAP), with Ca/P molar ratio equal to 1.50, has been synthesised and impregnated with different amounts of Pd (0.5-2%). The Pd(x)/HAP system has been thoroughly characterised (using BET, XRD, TEM, UV-visible-NIR, FTIR, XPS, CO_2-TPD and NH_3-TPD techniques) and tested in the DCE oxidation reaction.

Two types of Pd species have been identified on the prepared samples: (i) a phase where palladium is incorporated in the structure of the hydroxyapatite and adopting tetrahedral

coordination and (ii) large crystallites of PdO encapsulated by segregated HAP particles.

In DCE oxidation reaction the Pd(x)/HAP system has shown an activity comparable to that of a conventional system (Pd/alumina). However, the former has proved that it is highly selective towards the production of oxygenated products (CO_x (CO_2 and CO)). Notably, in contrast to the traditional supports behaviour, the DCE oxidation does not yield VC intermediate product over Pd(x)/HAP. This catalytic behaviour has been related to the moderate acidity of HAP compared to that of alumina together with its interaction with the Pd active phase. This report, then, considers that Pd(x)/HAP could be presented as a good alternative to those reported in the available literature. Concerning the determination of the active phases, the Pd^{2+} ions strongly interacting with HAP support have proved higher activity. By contrast, due to their inaccessibility to the gas mixture, the encapsulated Pd large particles can be practically considered inactive.

5. Acknowledgements

The financial support for this work provided by Ministerio de Economía y Competitividad (CTQ2015-73219-JIN (AEI/FEDER/UE), ENE2013-41187-R and CTQ2016-80253-R) and Gobierno Vasco (GIC IT-657-13) is gratefully acknowledged. Likewise, the technical support provided by SGIker (UPV/EHU) is gratefully acknowledged.

6. References

1. A. Aranzabal, B. Pereda-Ayo, M.P. González-Marcos, J.A. González-Marcos, R. López-Fonseca, J.R. González-Velasco, Chem. Pap. 68 (2014) 1169-1186.

2. Z. Boukha, J. González-Prior, B.d. Rivas, J.R. González-Velasco, R. López-Fonseca, J.I. Gutiérrez-Ortiz, Appl. Catal. B. 190 (2016) 125-136.

3. J.R. González-Velasco, A. Aranzabal, J.I. Gutiérrez-Ortiz, R. López-Fonseca, M.A. Gutiérrez-Ortiz, Appl. Catal. B. **19 (1998)** 189-197.

4. D. Comandella, S. Woszidlo, A. Georgi, F.-. Kopinke, K. Mackenzie, Appl. Catal. B. 186 (2016) 204-211.

5. E. Diaz, M. Cebrian, A. Bahamonde, M. Faraldos, A.F. Mohedano, J.A. Casas, J.J. Rodriguez, Catal. Today 266 (2016) 168-174.

6. Y. Han, C. Liu, J. Horita, W. Yan, Appl. Catal. B. 188 (2016) 77-86.

7. Y. Han, J. Sun, H. Fu, X. Qu, H. Wan, Z. Xu, S. Zheng, Appl. Catal. A. 519 (2016) 1-6.

8. M. Martin-Martinez, L.M. Gómez-Sainero, M.A. Alvarez-Montero, J. Bedia, J.J. Rodriguez, Appl. Catal. B. 132-133 (2013) 256-265.

9. R.M. Mironenko, O.B. Belskaya, V.S. Solodovnichenko, T.I. Gulyaeva, Y.G. Kryazhev, V.A. Likholobov, Kinet. Catal. 57 (2016) 229-233.

10. M. Gallastegi-Villa, A. Aranzabal, Z. Boukha, J.A. González-Marcos, J.R. González-Velasco, M.V. Martínez-Huerta, M.A. Bañares, Catal. Today 254 (2015) 2-11.

11. N. Blanch-Raga, A.E. Palomares, J. Martínez-Triguero, S. Valencia, Appl. Catal. B. 187 (2016) 90-97

12. J. González-Prior, R. López-Fonseca, J.I. Gutiérrez-Ortiz, B. de Rivas, Appl. Catal. B. 199 (2016) 384-393.

13. P. Sun, W. Wang, X. Dai, X. Weng, Z. Wu, Appl. Catal. B. 198 (2016) 389-397.

14. A. Tang, L. Hu, X. Yang, Y. Jia, Y. Zhang, Catal. Commun. 82 (2016) 41-45.

15. P. Yang, S. Zuo, Z. Shi, F. Tao, R. Zhou, Appl. Catal. B. 191 (2016) 53-61.

16. C. Zhang, C. Wang, S. Gil, A. Boreave, L. Retailleau, Y. Guo, J.L. Valverde, A. Giroir-Fendler, Appl. Catal. B. 201 (2017) 552-560.

17. R. Rachapudi, P.S. Chintawar, H.L.J. Greene, J. Catal. 185 (1999) 58-72.

18. B. Miranda, E. Diaz, S. Ordonez, A. Vega, F.V. Diez, Appl. Catal. B. 64 (2006) 262-271.

19. S. Pitkäaho, L. Matejova, S. Ojala, J. Gaalova, R.L. Keiski, Appl. Catal. B. 113-114 (2012) 150-159.

20. R. López-Fonseca, J.I. Gutiérrez-Ortiz, J.R. González-Velasco, Appl. Catal. A. 271 (2004) 39-46.

21. J.-. Lamonier, T.B. Nguyen, M. Franco, S. Siffert, R. Cousin, Y. Li, X.Y. Yang, B.-. Su, J.-. Giraudon, Catal. Today 164 (2011) 566-570.

22. A. Michalik-Zym, R. Dula, D. Duraczyńska, J. Kryściak-Czerwenka, T. Machej, R.P. Socha, W. Włodarczyk, A. Gaweł, J. Matusik, K. Bahranowski, E. Wisła-Walsh, L. Lityńska-Dobrzyńska, E.M. Serwicka, Appl. Catal. B. 174-175 (2015) 293-307.

23. Z. Boukha, J.L. Ayastuy, J.R. González-Velasco, M.A. Gutiérrez-Ortiz, Appl. Catal. B. 201 (2017) 189-201.

24. Z. Boukha, M. Kacimi, M.F.R. Pereira, J.L. Faria, J.L. Figueiredo, M. Ziyad, Appl. Catal. A. 317 (2007) 299-309.

25. Z. Boukha, M. Kacimi, M. Ziyad, A. Ensuque, F. Bozon-Verduraz, J. Mol. Catal. A. 270 (2007) 205-213.

26. Y. Matsumura, H. Kanai, J.B. Moffat, J. Mol. Catal. A. 115 (1997) L229-L232

27. R.S. Weber, J. Catal. 151 (1995) 470-474.

28. B. De Rivas, R. López-Fonseca, C. Jiménez-González, J.I. Gutiérrez-Ortiz, J. Catal. 281 (2011) 88-97.

29. A. Aranzabal, J.A. González-Marcos, J.L. Ayastuy, J.R. González-Velasco, Chem. Eng. Sci. 61 (2006) 3564-3576

30. M.M.R. Feijen-Jeurissen, J.J. Jorna, B.E. Nieuwenhuys, G. Sinquin, C. Petit, J. Hindermann, Catal. Today 54 (1999) 65-79.

31. T Yu, H Shaw, R.J Farrauto, ACS Symp. Ser. 495 (1992) 141.

32. B. de Rivas, R. Lopez-Fonseca, J.R. Gonzalez-Velasco, J.I. Gutierrez-Ortiz, J. Mol. Catal. Catal. A. 278 (2009) 181-188.

33. J. Zhou, L. Zhao, Q. Huang, R. Zhou, X. Li, Catal. Lett., 127 (2009) 277-284.

34. J.R. González-Velasco, R. López-Fonseca, A. Aranzabal, J.I. Gutiérrez-Ortiz, P. Steltenpohl, Appl. Catal. B. 24 (2000) 233-242.

35. B. Ramachandran, H.L. Greene, S. Chatterjee, Appl. Catal. B. 8 (1996) 157-182.

36. P. Jones, J.A. Hockey, Trans. Faraday Soc. 67 (1971) 2679.

37. A. Rakai, D. Tessier, F. Bozon-Verduraz, New J. Chem. 16 (1992) 869-875.

38. E.A. Sales, G. Bugli, A. Ensuque, M. De Jesus Mendes, F. Bozon-Verduraz, Phys. Chem. Chem. Phys. 1 (1999) 491-498.

39. J.A. Kurzman, M. Miao, R. Seshadri, J. Phys. Condens. Matter. 23 (2011) 1-12.

40. A. L. Guimarães, L. C. Dieguez, M. Schmal, J. Phys. Chem. B 107 (2003) 4311-4319.

41. M. Brun, A. Berthet, J.C. Bertolini, J Electron Spectrosc Relat Phenom. 104 (1999) 55-60.

42. A.J. Forman, J. Park, W. Tang, Y.-. Hu, G.D. Stucky, E.W. McFarland, ChemCatChem 2 (2010) 1318-1324.

43. L. Silvester, J.-. Lamonier, R.-. Vannier, C. Lamonier, M. Capron, A.-. Mamede, F. Pourpoint, A. Gervasini, F. Dumeignil, J. Mater. Chem. A. 2 (2014) 11073-11090.

44. B.R. Powell, S.E. Whittington, J. Catal. 81(2) (1983) 382-393.

45. H.P. Sun, X.P. Pan, G.W. Graham, H. Jen, R.W. McCabe, S. Thevuthasan, Appl. Phys. Lett. 87(20) (2005) 1-3.

CAPTIONS FOR TABLES AND FIGURES

Table 1 Catalytic data in DCE oxidation over Pd(x)/HAP samples.

Table 2 Textural properties of the fresh and used Pd(x)/HAP samples.

Table 3 XRD, XPS and ICP data for the prepared Pd(x)/HAP catalysts.

Table 4 Acid-base properties for the Pd(x)/HAP catalysts.

Fig. 1 Activity of the Pd(x)HAP catalysts in DCE oxidation as a function of temperature.

Fig. 2 Pseudo-first order fit for the DCE oxidation experimental data over the Pd(x)/HAP catalysts.

Fig. 3 Distribution of DCE oxidation products over Pd(x)/HAP catalysts.

Fig. 4 DCE conversion and selectivity to CO_2 and CO over Pd(0.5)/HAP catalyst at 375 °C as a function of time on stream.

Fig. 5 TEM micrographs of (a) Pd(0.5)/HAP, (b) Pd(1)/HAP, (c) Pd(2)/HAP and (d-e) HRTEM images of Pd(2)/HAP sample.

Fig. 6 XRD patterns of the Pd(x)/HAP fresh catalysts and Pd(x)/HAP-u catalysts used in DCE oxidation.

Fig. 7 FTIR spectra of Pd(x)/HAP calcined at 500 ºC.

Fig. 8 UV-Visible-NIR spectra of the (a) fresh and (b) used Pd(x)/HAP catalysts.

Fig. 9 XPS spectra of Pd 3d5/2 region for Pd(x)/HAP catalysts

Fig. 10 CO_2-TPD profiles of the Pd(x)/HAP catalysts.

Fig. 11 NH_3-TPD profiles of the Pd(x)/HAP catalysts.

Catalyst	T_{10},ºC	T_{50},ºC	T_{90}, ºC	$mol_{DCE}\ g^{-1}\ s^{-1}$ (x 10^{9}) 275 ºC	$mol_{DCE}\ m^{-2}\ s^{-1}$ (x 10^{10}) 275 ºC	TOF, $mol_{DCE}\ mol_{Pd}^{-1} s^{-1}$ (x 10^{4}) 275 ºC	E_a, kJ mol^{-1} (200-275 ºC)
HAP	405	500	-	6.8	1.3	-	90.0
Pd(0.5)/HAP	275	350	415	47.5	9.9	10.1	59.2
Pd(1)/HAP	275	340	410	47.0	9.8	5.0	69.8
Pd(2)/HAP	280	350	450	37.2	7.7	2.0	70.6

Table 1

		Fresh catalysts			Used catalysts		
Catalysts	Pd, wt.%	S_{BET}, $m^2 g^{-1}$	Pore volume, $cm^3 g^{-1}$	Pore size, nm	S_{BET}, $m^2 g^{-1}$	Pore volume, $cm^3 g^{-1}$	Pore size, nm
HAP	0.00	52.0	0.45	30.3	46.5	0.40	30.0
Pd(0.5)/HAP	0.56	48.3	0.39	28.0	48.0	0.42	31.8
Pd(1)/HAP	0.99	48.0	0.40	30.0	48.7	0.42	31.2
Pd(2)/HAP	2.05	47.8	0.37	29.0	41.2	0.32	29.8

Table 2

Catalysts	XRD			XPS						ICP	
	(a±0.01), Å	(c±0.002), Å	V, Å3	Pd $3d_{5/2}$, eV	O 1s, eV	Ca 2p, eV	P 2p, eV	Ca/P	Pd/P	Ca/P	Pd/P
HAP	9.3616	6.8116	517	-	530.6	346.9	133.7	1.50	0.000	1.50	0.000
Pd(0.5)/HAP	9.3646	6.8105	517.2	337.0	530.3	347.1	133.2	1.39	0.010	1.48	0.009
Pd(1)/HAP	9.3735	6.8181	518.8	337.0	530.3	347.2	133.6	1.45	0.013	1.50	0.017
Pd(2)/HAP	9.3942	6.8093	520.4	336.4	530.3	347.2	133.3	1.47	0.022	1.49	0.034

Table 3

	Acidity		Basicity	
Catalysts	$\mu mol_{NH3}\ g^{-1}$	$\mu mol_{NH3}\ m^{-2}$	$\mu mol_{CO2}\ g^{-1}$	$\mu mol_{CO2}\ m^{-2}$
HAP	90.0	1.7	133	2.6
Pd(0.5)/HAP	64.9	1.3	72	1.5
Pd(1)/HAP	73.5	1.5	58	1.2
Pd(2)/HAP	70.6	1.5	35	0.7

Table 4

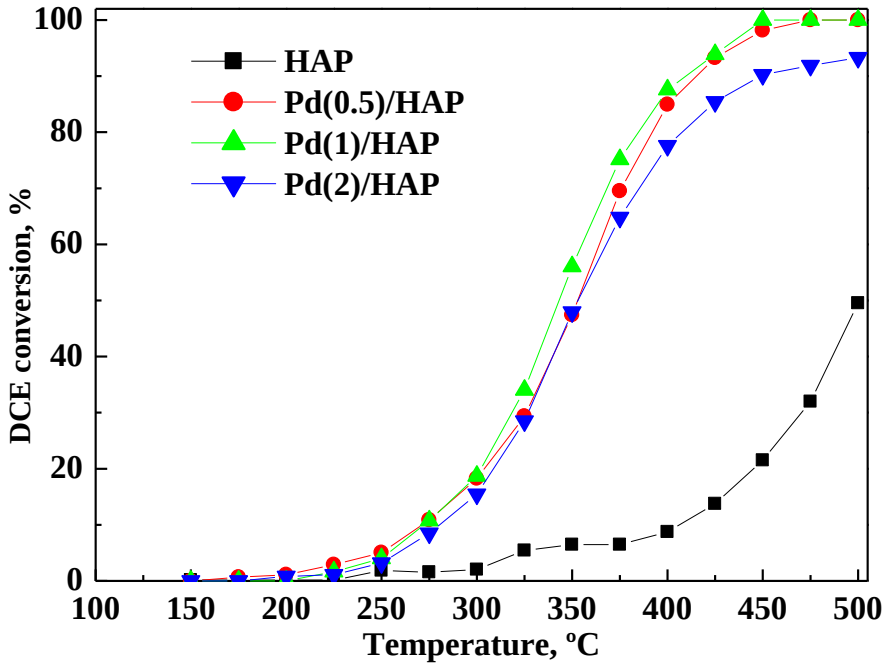

Figure 1.

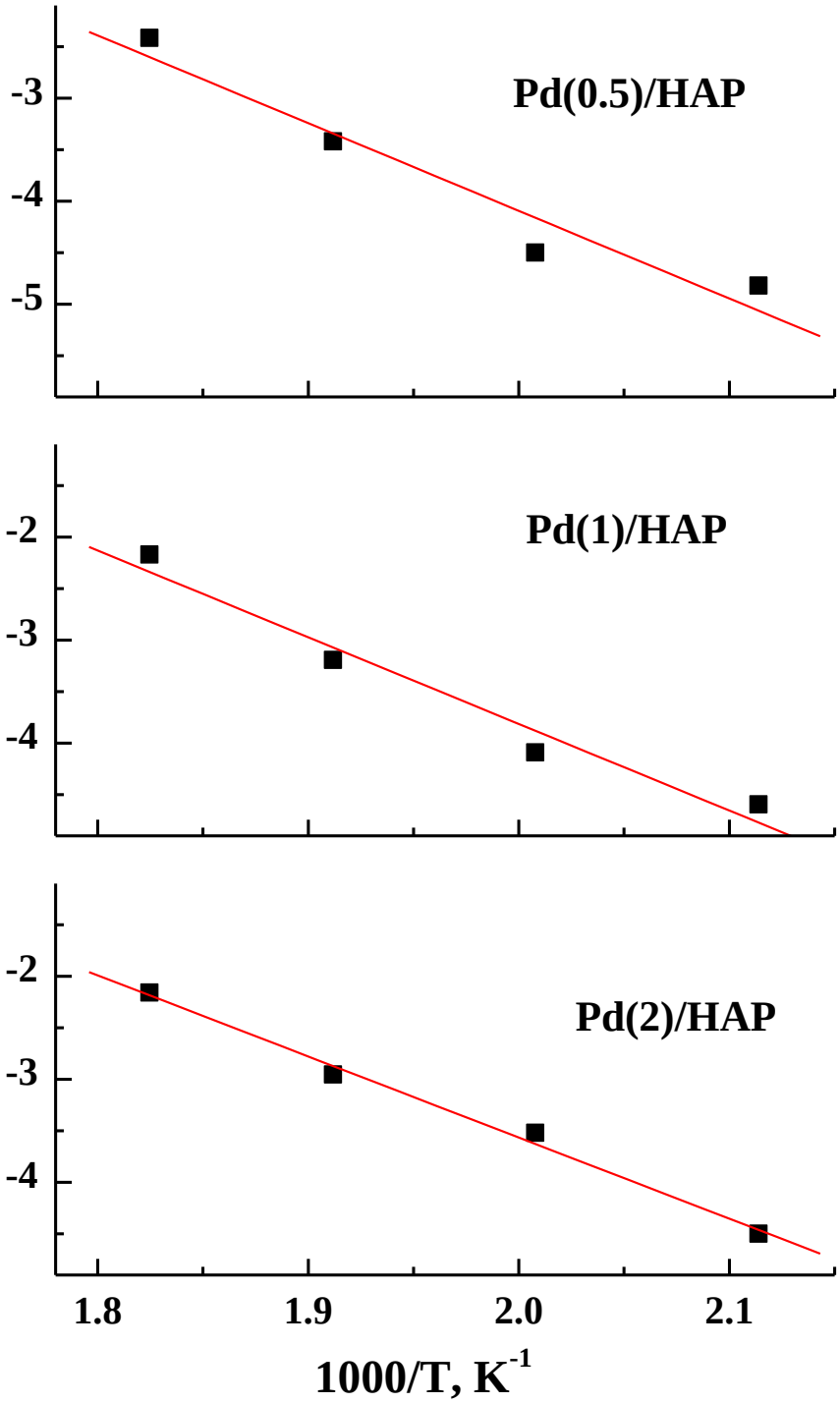

Figure 2.

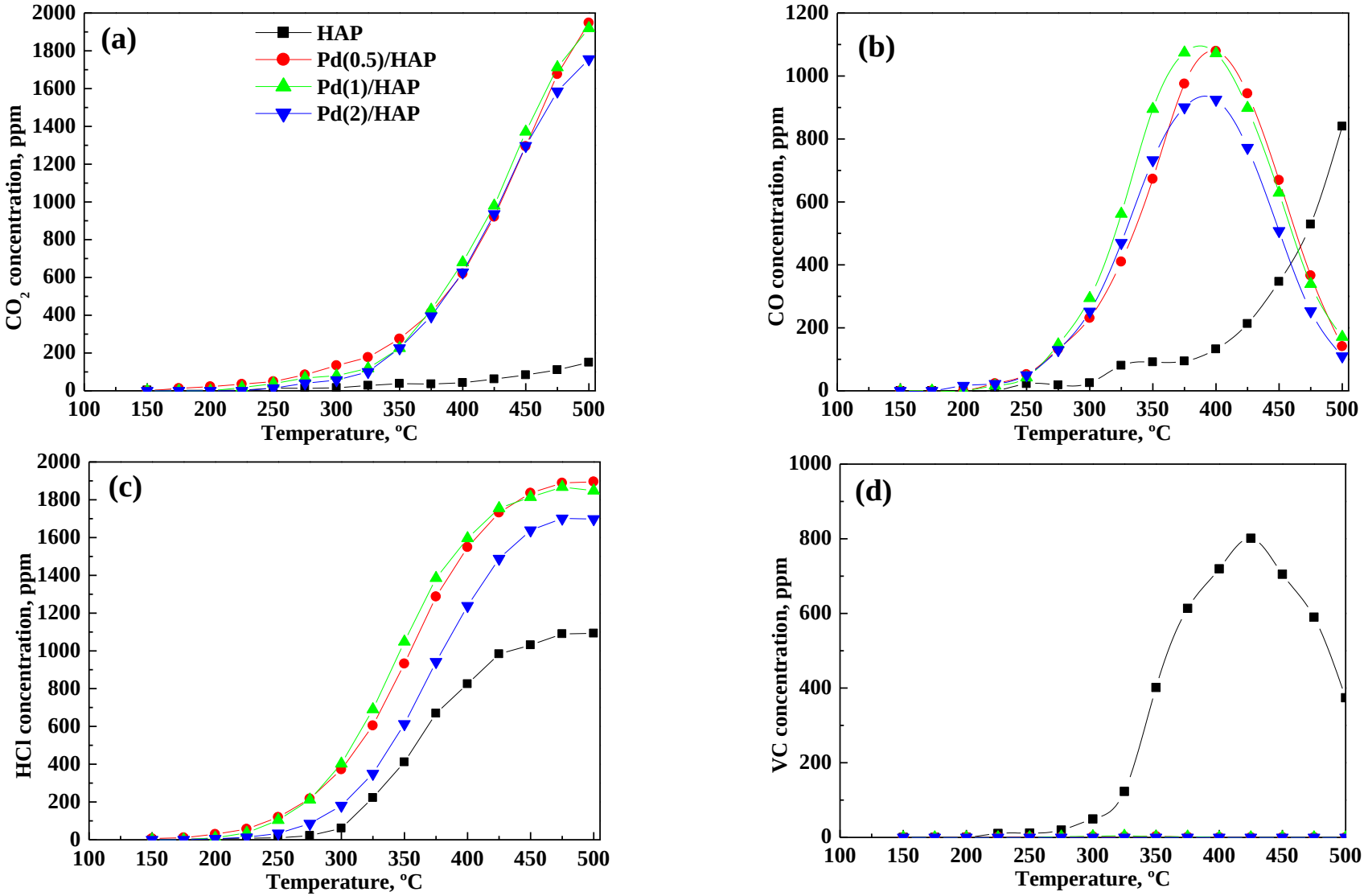
(a)
HAP
Pd(0.5)/HAP
Pd(1)/HAP
Pd(2)/HAP
CO2 concentration, ppm
Temperature, °C
(b)
CO concentration, ppm
Temperature, °C
(c)
HCl concentration, ppm
Temperature, °C
(d)
VC concentration, ppm
Temperature, °C

Figure 3.

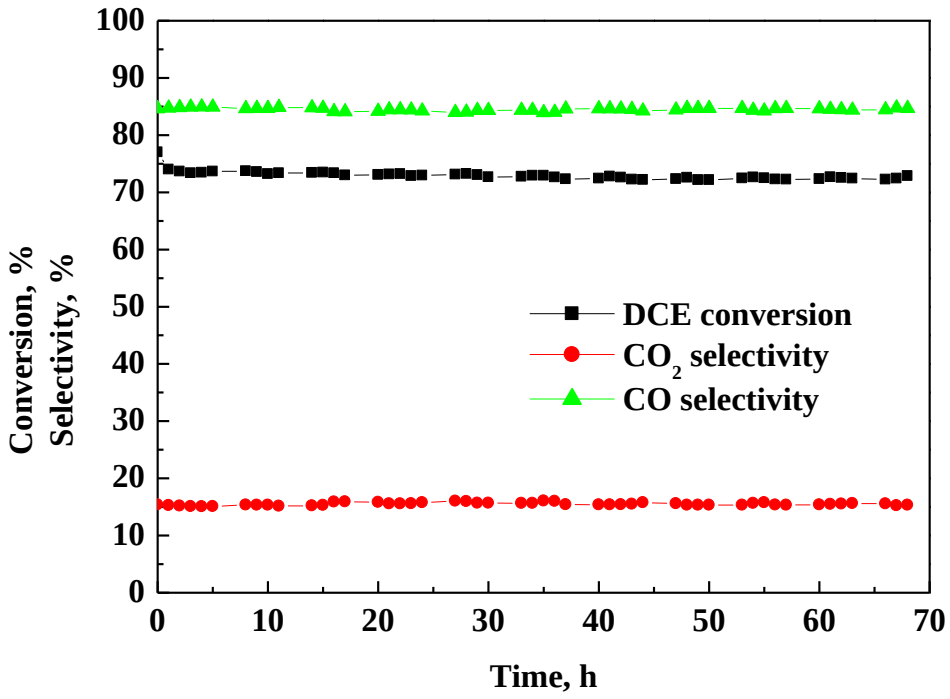
Conversion, %
Selectivity, %
Time, h
DCE conversion
CO2 selectivity
CO selectivity
0
10
20
30
40
50
60
70
80
90
100

Figure 4.

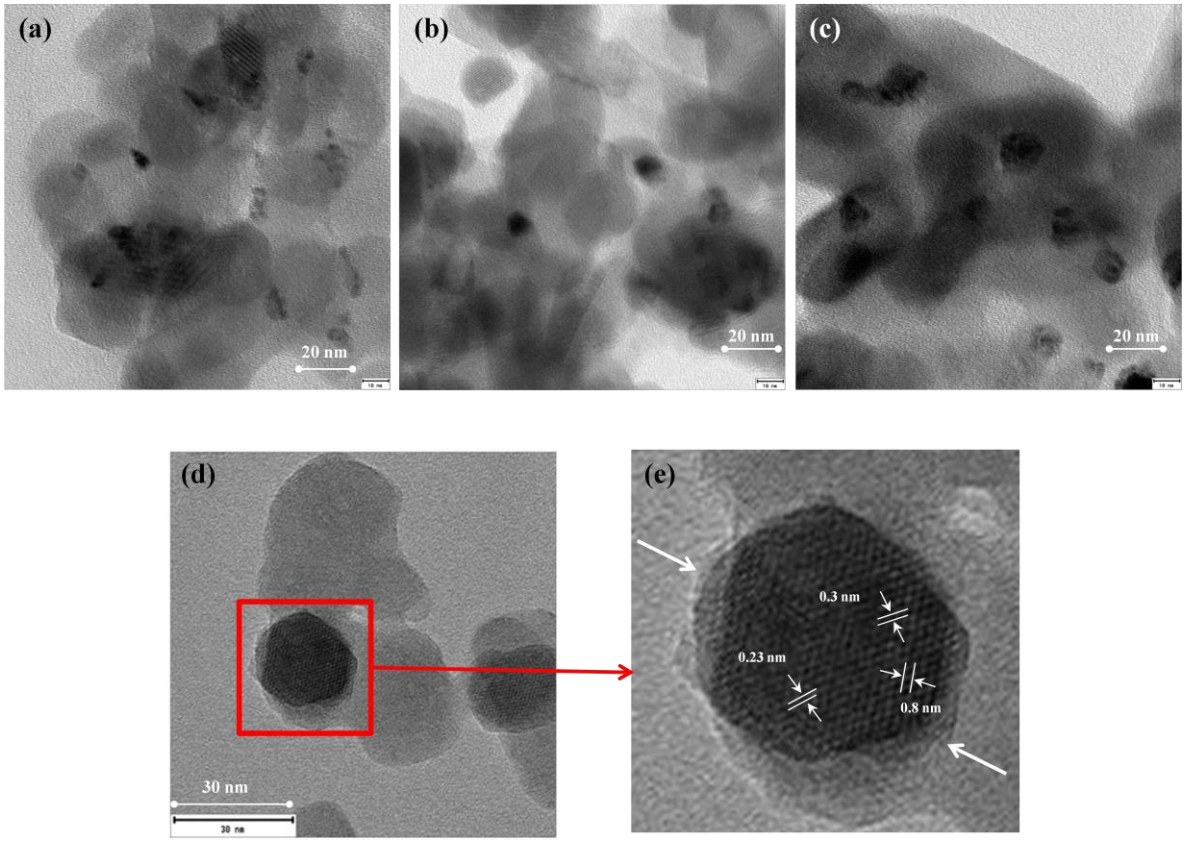

Figure 5

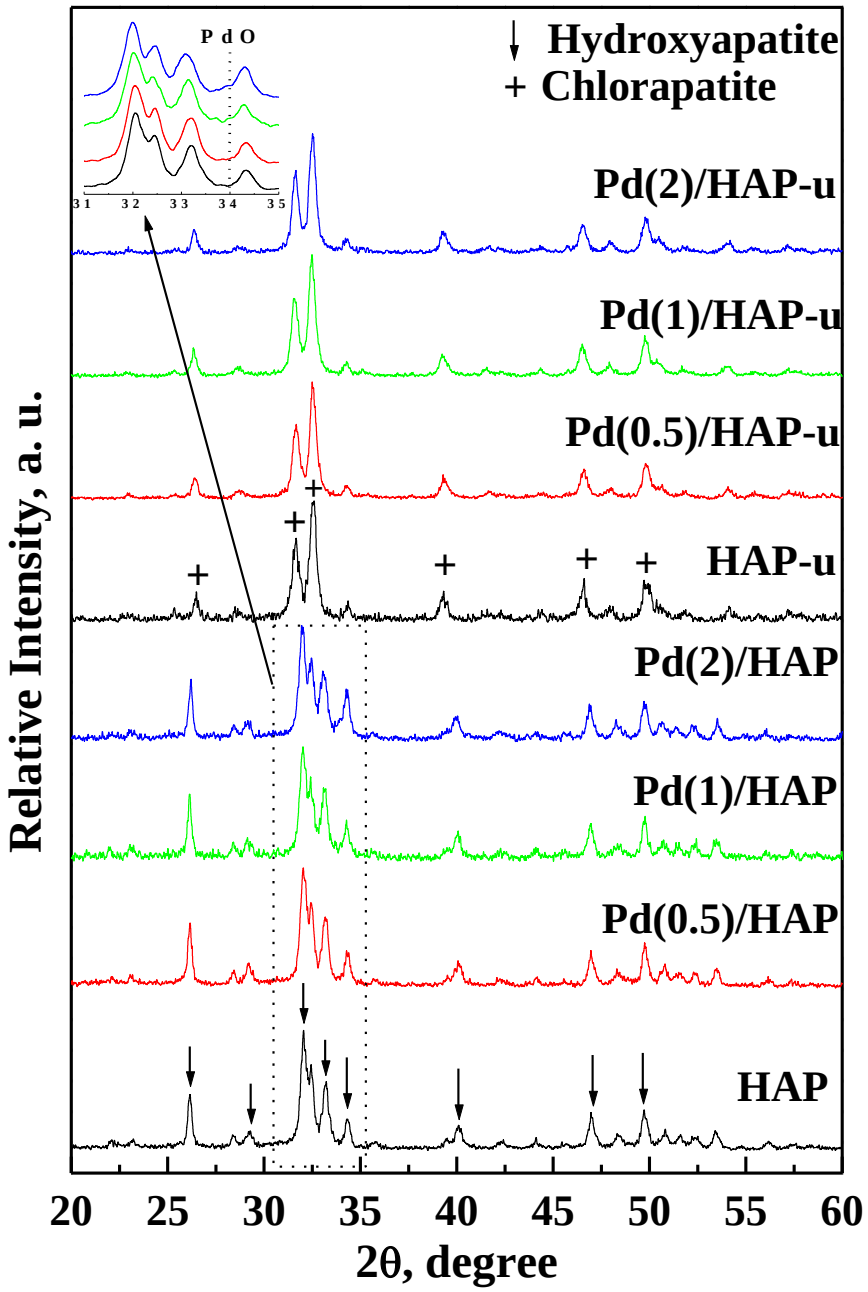
P d O
31
32
33
34
35
↓ Hydroxyapatite
+ Chlorapatite
Pd(2)/HAP-u
Pd(1)/HAP-u
Pd(0.5)/HAP-u
HAP-u
Pd(2)/HAP
Pd(1)/HAP
Pd(0.5)/HAP
HAP
Relative Intensity, a. u.
20
25
30
35
40
45
50
55
60
2θ, degree

Figure 6

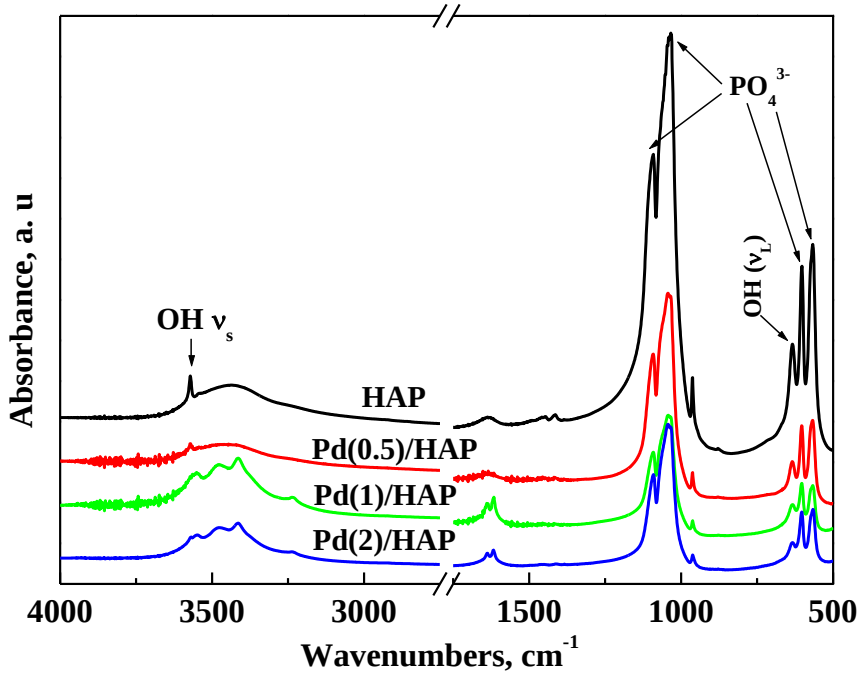
Absorbance, a. u
OH ν s
HAP
Pd(0.5)/HAP
Pd(1)/HAP
Pd(2)/HAP
PO 4 3-
OH (ν L)
4000
3500
3000
1500
1000
500
Wavenumbers, cm-1

Figure 7

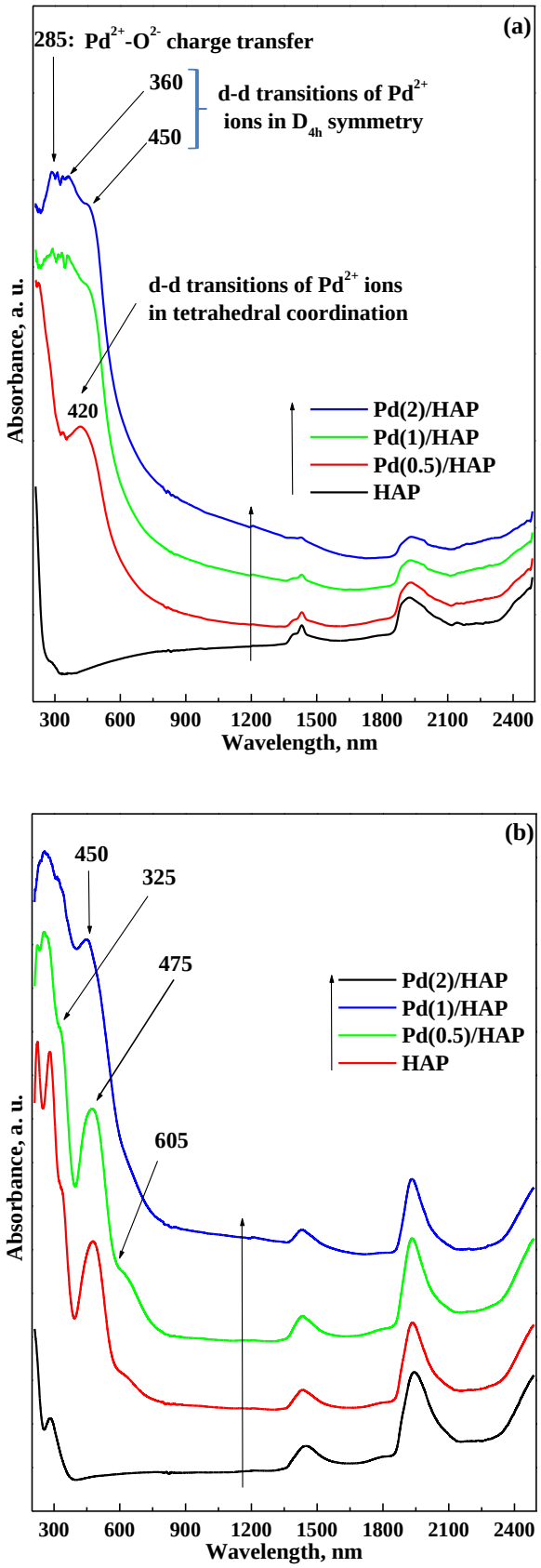
(a)
285: Pd2+-O2- charge transfer
360
450
d-d transitions of Pd2+
ions in D4h symmetry
d-d transitions of Pd2+ ions
in tetrahedral coordination
420
Pd(2)/HAP
Pd(1)/HAP
Pd(0.5)/HAP
HAP
Absorbance, a. u.
300 600 900 1200 1500 1800 2100 2400
Wavelength, nm
(b)
450
325
475
605
Pd(2)/HAP
Pd(1)/HAP
Pd(0.5)/HAP
HAP
Absorbance, a. u.
300 600 900 1200 1500 1800 2100 2400
Wavelength, nm

Figure 8

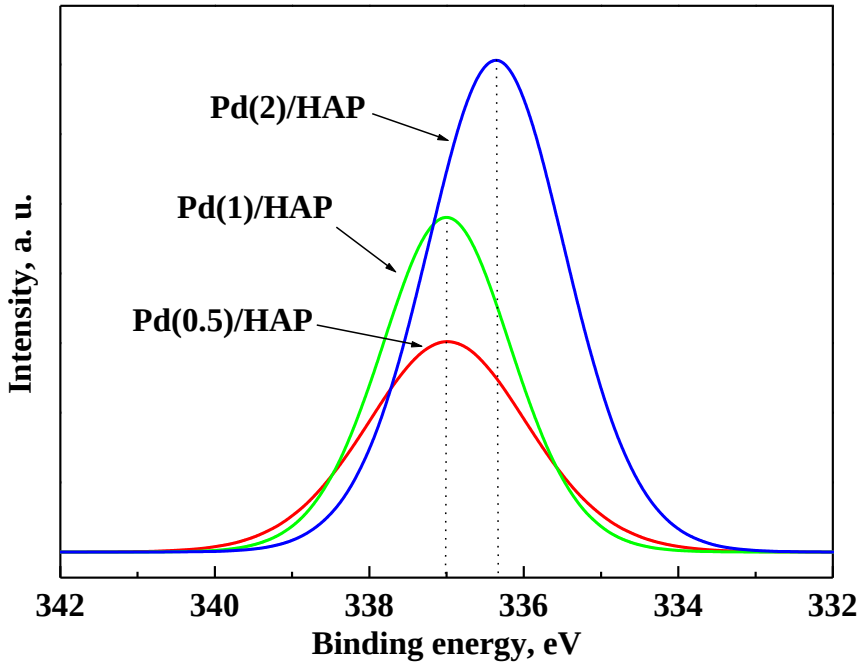
Pd(2)/HAP
Pd(1)/HAP
Pd(0.5)/HAP
Intensity, a. u.
342
340
338
336
334
332
Binding energy, eV

Figure 9

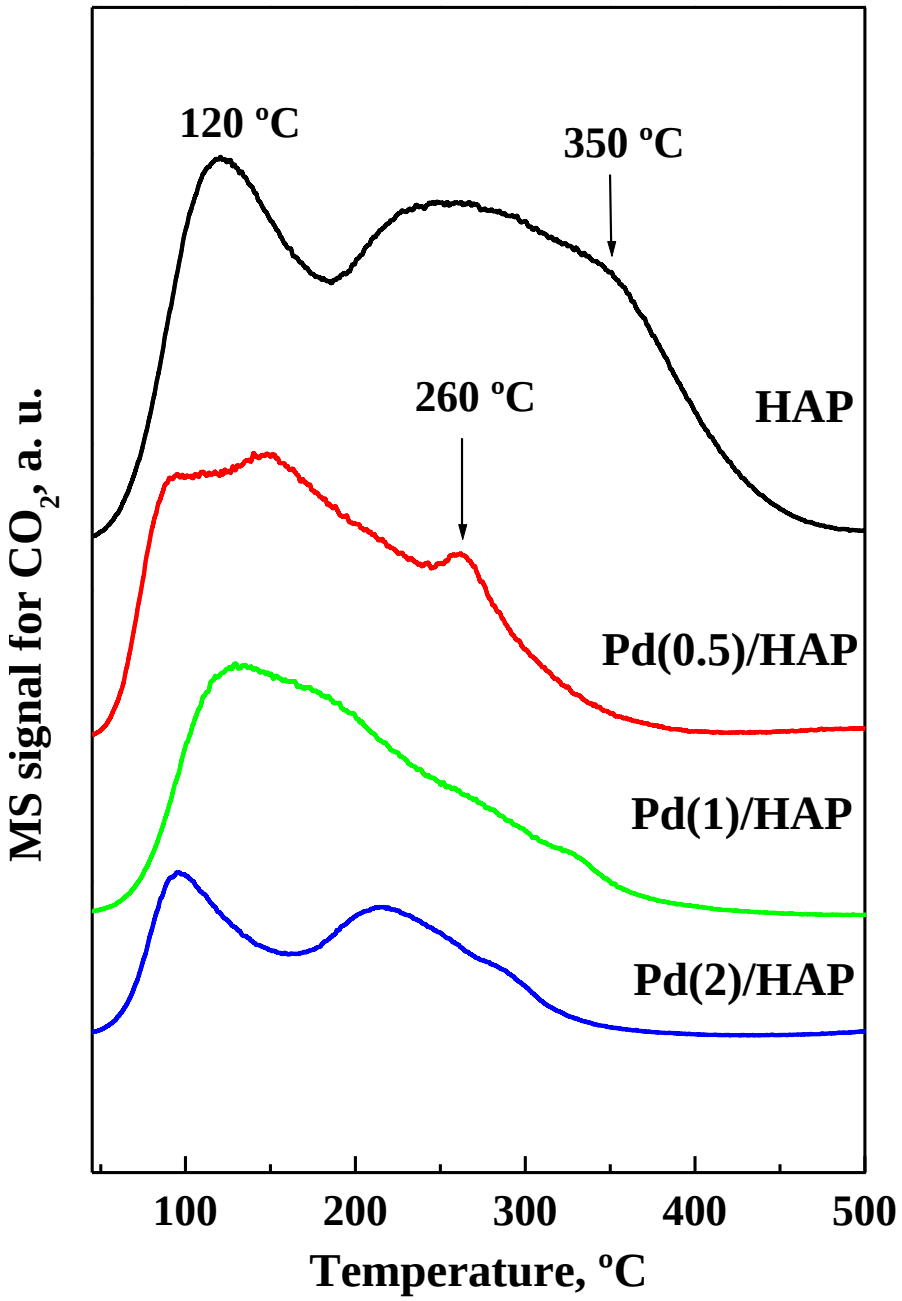
120 ºC
350 ºC
260 ºC
HAP
Pd(0.5)/HAP
Pd(1)/HAP
Pd(2)/HAP
MS signal for CO_2, a. u.
100
200
300
400
500
Temperature, ºC

Figure 10

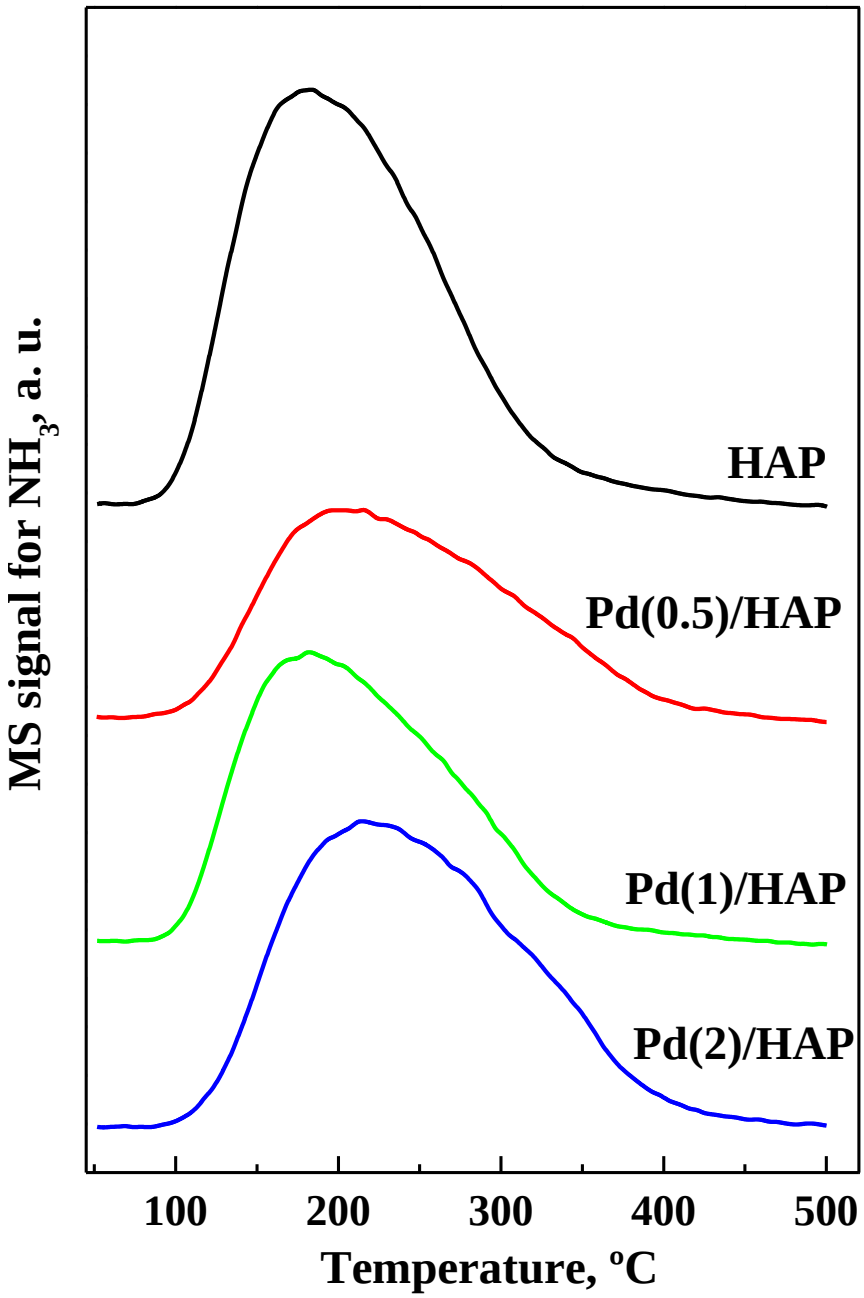
MS signal for NH3, a. u.
HAP
Pd(0.5)/HAP
Pd(1)/HAP
Pd(2)/HAP
100
200
300
400
500
Temperature, °C

Figure 11

*Graphical Abstract

GRAPHICAL ABSTRACT

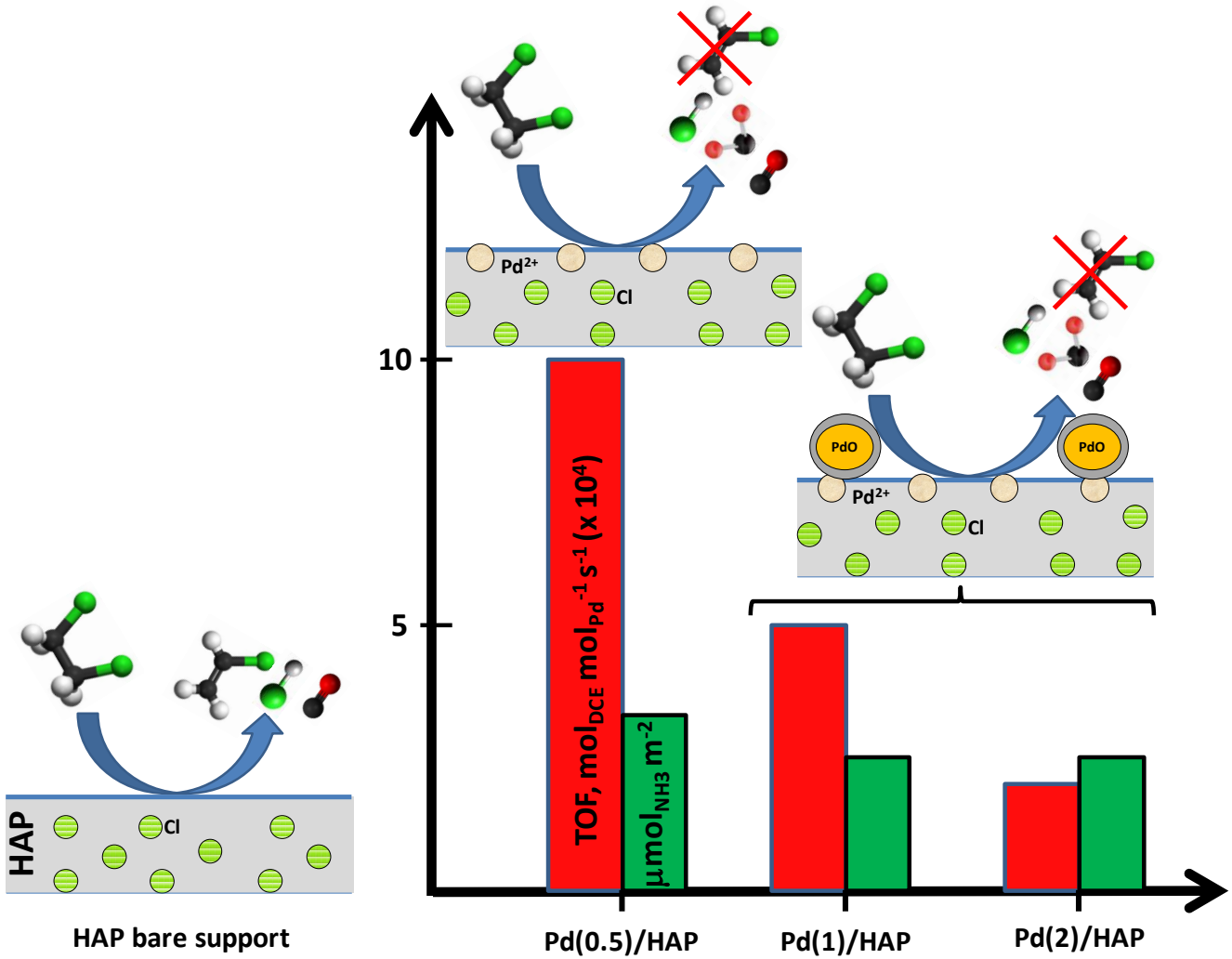

HIGHLIGHTS – BULLET POINTS

HAP supported Pd catalysts are synthesised, characterised and tested in DCE oxidation.

Two types of Pd species have been identified on the prepared samples.

The Pd catalysts have been successfully tested in the DCE oxidation.

The Pd(x)/HAP catalysts are not selective towards VC intermediate production.

The Pd^{2+} species strongly interacting with HAP support have proved higher activity.